The Failure of the Immutable Emissivity Assumption (#2101)

Michael S. Ramsey[1] & Alan R. Gillespie[2]

[1] Dept. of Geology and Planetary Science, University of Pittsburgh, Pittsburgh, PA

[2] Dept. of Earth and Space Sciences, University of Washington, Seattle, WA

INTRODUCTION:

Infrared emissivity is a fundamental property commonly used to identify the composition of planetary surfaces and atmospheres [1]. Numerous detection and mapping methods have been developed over the years that rely on spectral libraries as truth in order to identify these constituents in orbital thermal infrared (TIR) datasets [2-3]. For many common scenarios, this approach works assuming the complicating factors and model limitations are well understood. Here, we explore a subset of the vast array of situations where emissivity can no longer be assumed constant and the use of spectral libraries to map planetary surfaces could be problematic.

For a blackbody material with an emissivity of unity at all wavelengths, the emitted radiance follows a Planck distribution (Eqn. 1) and is the maximum possible for a given temperature (Fig. 1). However, vibrations in the atomic structure of most materials give rise to discrete regions where the emissivity is less than one (Fig. 2). Emissivity therefore can be defined as the fractional representation of the amount of energy emitted from a surface at a given temperature compared to the energy from a blackbody at the same temperature. These absorption bands have been used to identify the constituents of the emitting surface whether in the laboratory, in the field, from the air, or from orbit (Fig. 3).

$$L(\lambda, T) = \varepsilon_\lambda \left\{ \frac{(c_1 \lambda^{-5})}{\exp(c_2 / \lambda T) - 1} \right\} \qquad (1)$$

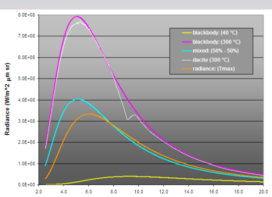

Figure 1. Thermal infrared (TIR) radiance curves of blackbodies and a dacite showing the spectral absorptions at ~ 5.2 and 9.2 microns. If a surface is composed of two materials having two temperatures (40° C and 300° C), the resulting radiance no longer follows Planck behavior (cyan vs. orange spectra). This non-linearity results in errors to the retrieved emissivity spectrum because of the assumption of Planck behavior (Fig. 2).

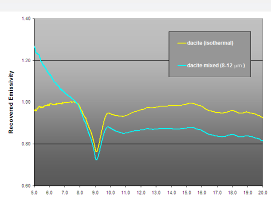

Figure 2. TIR emission spectra retrievals of the dacite sample (Fig. 1). Isothermal sample (yellow) showing an accurate retrieval with maximum emissivity values near unity and the correct depth of the main absorption feature. Non-isothermal sample (cyan) similar to the mixed spectrum shown in Fig 1. Note the lower than expected emissivity at longer wavelengths. A similar emissivity depression can be caused by the "Planck Effect", which results when the apparent emissivity is calculated by the ratio of the Planck radiance integrated over a narrow band to a broad band and normalizing to an emissivity of unity.

MEASUREMENTS:

Where trying to measure emissivity uniquely, one must also know the surface kinetic temperature (or the emissivity at one wavelength). This constraint has been largely overcome by a variety of techniques including detailed laboratory calibration [4] or measuring the infrared reflectance, which is inversely related to the emissivity and much less dependant on temperature (Fig. 4). Once measured, numerous modeling approaches have been developed to deconstruct the emissivity spectrum in order to extract other properties such as compositional mixing (Fig. 3), grain size of the surface (Fig. 5), thermal inertia (Fig. 6). These rely on the assumption that emissivity, where sampled accurately, remains unchanged, which may not always be true.

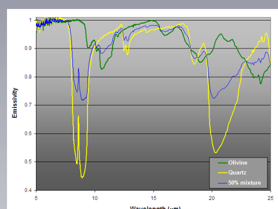

Figure 3. Laboratory emissivity spectra derived from isothermal mineral particulates (500 μm). Quartz and olivine have distinct absorption features that combine linearly if the particulates are mixed (here at 50% each). Assuming no other complications (i.e., thermal mixing, different particle sizes, etc.) linear deconvolution models can be applied to such mixed spectra to derive mineral type and percentage [5].

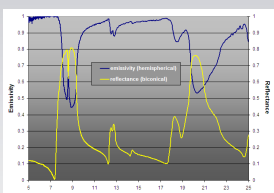

Figure 4. TIR spectra of quartz acquired in hemispherical emission using the approach of [4] and biconical reflectance (taken from the JHU spectral library). Although biconical reflectance differs slightly from emissivity *(e.g., the behavior at wavelengths prior to a large absorption bands)*, generally reflectance can be converted to emissivity using Kirkoff's Law [ε = 1 - R]. However, most remote sensing systems acquire emitted radiance and therefore the interdependency of emissivity and temperature must be considered.

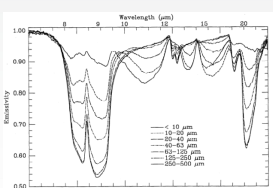

Figure 5. Grain size effects on emissivity spectra for quartz particulates (from [5]). The large bands at 1250, 775, and 500 wavenumber have a reduction in contrast with decreasing particle size because of the large absorption coefficient [k(λ)] and therefore the dominance of specular reflection in these regions. Increased contrast occurs at 900, 725, and 625 wavenumber, where volume scattering dominates due to the low k(λ) values.

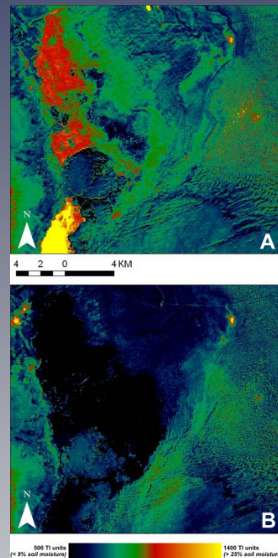

Figure 6. Thermal inertia images of the White Sands dune field derived from the ASTER sensor [6]. Day/night thermal infrared and visible/short-wave infrared albedo data were used to create the images. Thermal inertia was converted to soil moisture using a numerical approximation. Accurate ground temperature retrievals were highly dependant upon proper knowledge of the variable emissivity of the ground surface. Note the dramatic change in soil moisture values; the lower soil moisture seen in [B] preceded a large dust emission event by several days. [A] 27 April 2007. [B] 12 March 2008. Approximately 36 hours separated the day/night overpasses.

COMPLICATIONS:

The assumption of immutable emissivity has been shown to be false for certain situations and in fact may not be strictly true for many remote measurements. For example, surface coatings, temperature gradients/mixing, and particle-size variations (Fig. 5), (all common in planetary applications) dramatically alter the emissivity spectrum of common minerals.

More recently, micron-scale surface roughness [7] and cavity radiation at larger roughness scales [8] have also been shown to decrease the contrast of the emissivity features. This effect has been used to model the percentage of vesicles in extrusive/explosive volcanic products (Figs. 7 & 8) and to understand the importance of surface topography using radiosity models (Figs. 9 & 10).

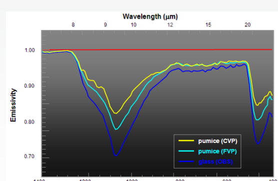

Figure 7. Effects of micron-scale roughness on TIR emissivity spectra [7]. As the number and connectedness of surface vesicles increases from finely vesicular pumice (FVP) to coarsely vesicular pumice (CVP), the emission increases linearly. Using a deconvolution model with two end-members: obsidian glass (OBS) and blackbody, the percentage of vesicles in the two types of pumice (coarse and fine) was accurately determined.

COMPLICATIONS (con't):

Furthermore, for measurements made over thermally heterogeneous surfaces, the non-linear mixing of temperatures will greatly alter the final emissivity spectrum making both quantitative analyses and accurate correction difficult. This was observed by [9] on active flows in Hawaii (Fig. 11). The question of whether this lowering of emissivity is a real phenomena or a result of the "Planck Effect" was later addressed by using a thermal IR camera and thermocouple [10]. However, small-scale temperature variations due to crust formation, etc. could not be constrained using this measurement approach. The uncertainty was later resolved by [11] using a novel micro-furnace to track the change in emissivity with temperature as silicate samples underwent melting (Fig. 12).

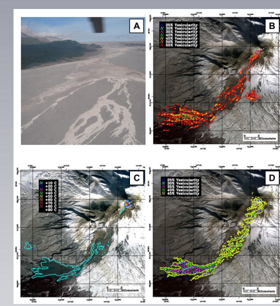

Figure 8. Surface temperature and modeled surface vesicularity changes derived from ASTER TIR data acquired in March 2005. Note the reduction in surface vesicularity of the pyroclastic flow deposit over the two-week period. [A] Helicopter-based photograph of the 27 February 2005 pyroclastic flow deposit (taken by M. Ramsey on 25 August 2005). [B] 12 March 2005 vesicularity. [C] 29 March 2005 temperature. [D] 29 March 2005 vesicularity.

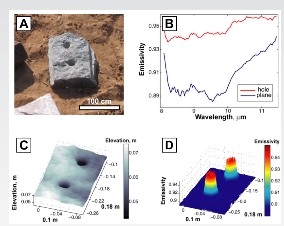

Figure 9. Impact of surface topography on derived emissivity. [A] Norite rock with two drilled holes. [B] Field-based emissivity spectra of the rock using a TELOPS Inc. HgCdTe imaging spectrometer *(note the reduction in spectral contrast of the holes)*. [C] Micro digital elevation model (DEM) of the rock's upper surface. [D] Change in the derived emissivity due to the blackbody effect can be calculated using a radiosity model.

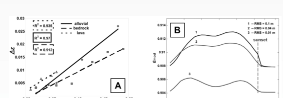

Figure 10. Effect of surface roughness on Δε [8]. [A] Change in emissivity for alluvial (◇), bedrock (□), and lava flow (△) surfaces. Value of ε used for the model calculations was 0.9, T = 300K. [B] Radiosity model of emissivity averaged over the course of a day for alluvial surfaces of different roughness in Death Valley. Note different time step after sunset.

SUMMARY:

Research by the authors into the response of emissivity with roughness, composition, mantling, and large temperature changes has verified the dramatic variability that occurs. The change of state (i.e., a structural phase changes as the material begins to melt) is particularly striking. Furthermore, small-scale changes may arise even at much lower temperatures, calling into question the accuracy and interpretability of emissivity at the percent level. Spectral effects due to eolian mantling and mixing on young lava flows on Mars can also be seen (Fig. 13). Data from the laboratory, field, and future TIR sensors (e.g., HyspIRI) should be carefully inspected prior to interpretations of TIR emissivity and temperature.

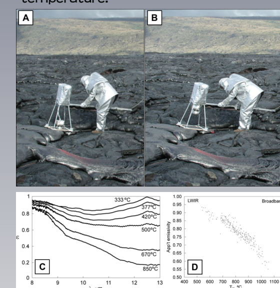

Figure 11. In-situ measurements of emissivity on molten basalt in Kilauea, Hawaii [9]. [A] Measurement device consisting of an FTIR instrument mated to a hemispherical collector *(electronics are housed in the upper part)*. [B] Instrument prior to deployment. [C] Spectra showing progressive decrease in emissivity at longer wavelengths with increasing temperature either due to the "Planck Effect" or a real change in emissivity with increasing temperature. [D] Broadband emissivity of all spectral measurements versus temperature.

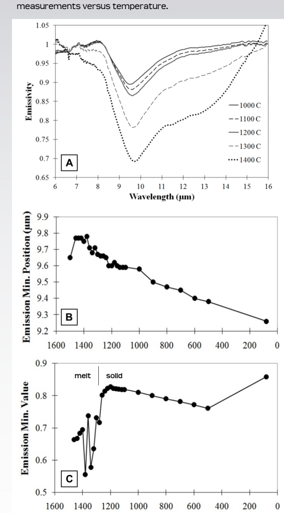

Figure 12. Results from the in-situ melting and laboratory spectral acquisition of a synthetic glass mixture (Ab50 + Qtz) [11]. [A] With increasing temperature, the emissivity is depressed by more than 35%. [B] The emissivity minimum position shifts linearly to longer wavelengths with temperature. [C] The emissivity minimum value also follows a linear increase with temperature until reaching the liquidus temperature (~ 1350 °C).

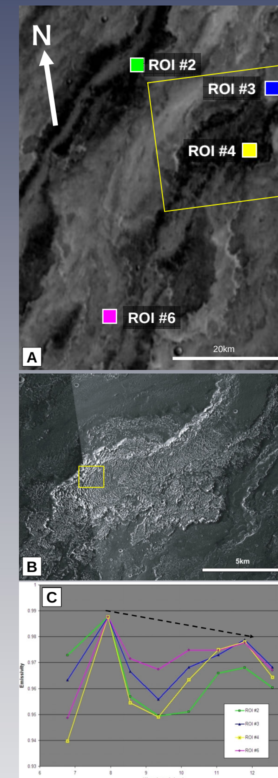

Figure 13: Diversity of the Arsia Mons (SW flank) flows [12]. [A] THEMIS temperature image (I07370003) with the locations and sizes of four regions of interest (ROI). ROI #2 and #4 were extracted from the more rugged (cooler) flows, whereas ROI #1 and #4 were from the lower albedo smoother flows. Yellow box indicates the area shown in [B]. [B] Full resolution CTX image mosaic of the Arsia Mons flow field centered at 121.50°W, 22.13°S showing the complex flow relationships and different flow morphologies *(i.e., bright/rugged and dark/smooth)*. [C] Spectra show a shorter wavelength absorption in ROI #3, #4, and #6 perhaps indicating a less mafic composition. Note also the long wavelength drop *(dashed arrow)*, which indicates thermal mixing at subpixel scales.

ACKNOWLEDGEMENTS:

This work was made possible by the NASA ASTER Science Team *(grant numbers NNX11AL29G to MR and JPL Subcontract 1318943/NM0711006 to AG)*, the NSF *(grant numbers: EAR0309631, EAR0711056, EAR1019558)*, and NASA THEMIS Science Team *(grant number NM0710630)* to MR. Thanks to I. Danilina for the data shown in Figures 9 & 10, and R. Lee for the data shown in Figure 12.

REFERENCES:

[1] Bandfield, J.L., et al. (2000) *Science, 110,* 1626-1630. [2] Christensen, P.R., et al. (2001) *JGR, 106,* 23873-23885. [3] Rodgers, A.D., et al. (2007) *JGR, 112,* E02004. [4] Ruff, S.W., et al. (1997) *JGR, 102,* 14899-14913. [5] Ramsey, M.S. & Christensen, P.R. (1998) *JGR, 103,* 577-596. [6] Scheidt, S., et al. (2010) *JGR, 115,* F02019. [7] Ramsey M.S. & Fink, J.H. (1999) *Bull. Volc. 61,* 32-39. [8] Danilina, I. (2011) Ph.D. Dissertation, Univ. of Washington. [9] Abtahi, A.A., et al. (2002) *AGU, #V71A-1263*. [10] Ramsey, M.S. & Lee, R.J. (2011) *IUGG XXV, #4184*. [11] Lee, R.J., et al. (2013) *JGR, (in review)*. [12] Ramsey, M.S. & Crown, D.A. (2010) *LPSC XLI, #1111.*